HOKKAIDO UNIVERSITY

Title	Anomalous Hanle effect considered in time-resolved measurements and numerical simulations
Author(s)	Yamamoto, S.; Kaji, R.; Adachi, S.
Citation	Physical Review B, 108(5), 054422 https://doi.org/10.1103/PhysRevB.108.054422
Issue Date	2023-08-16
Doc URL	https://hdl.handle.net/2115/90574
Rights	©[2023] American Physical Society
Type	journal article
File Information	PhysRevB.108.054422.pdf

Hokkaido University Collection of Scholarly and Academic Papers : HUSCAP

Anomalous Hanle effect considered in time-resolved measurements and numerical simulations

S. Yamamoto,[*] R. Kaji,[†] and S. Adachi[‡]
Division of Applied Physics, Hokkaido University, N13 W8, Kitaku, Sapporo 060-8628, Japan

(Received 2 February 2023; revised 23 June 2023; accepted 2 August 2023; published 16 August 2023)

In this study, the formation of a large in-plane nuclear field, known as the anomalous Hanle effect, in a self-assembled quantum dot was studied from both experimental and theoretical aspects. Time-resolved measurements of photoluminescence revealed that the buildup time of the nuclear field increased with increasing applied transverse magnetic field strength. Further, we found that inversion of the circular polarization degree of photoluminescence due to the excitation helicity reversal was completed on a timescale at least three orders of magnitude faster than the nuclear field buildup time. Accordingly, we reconsidered the previously proposed model for the anomalous Hanle effect. The alternatively developed model successfully explains the experimental results, suggesting that the in-plane component of the major principal axis of nuclear quadrupole interaction is essential for the generation of the anomalous Hanle effect.

DOI: 10.1103/PhysRevB.108.054422

I. INTRODUCTION

Hyperfine interaction (HFI), a spin exchange between a carrier and lattice nuclei, is enhanced owing to strong confinement of a carrier wave function in quantum dots (QDs). This enables the optical manipulation of the spin degrees of freedom of atomic nuclei via optically controllable electron spins. Therefore a semiconductor QD is a plausible candidate for establishing a platform that couples optical networks with qubits based on nuclear spins [1–3] and/or carrier spins [4,5] in solid state devices. For the application, it is necessary to gain a deeper understanding of the spin-coupled system composed of an electron and nuclei and find ways to control the nuclear spin polarization (NSP) more accurately.

So far, some remarkable topics related to NSP in QDs have been reported [6]. For example, the bistable response of NSP under a longitudinal magnetic field is one of the best-known phenomena observed in several kinds of QDs [7–10]. This phenomenon occurs when the optically induced NSP acts as an effective magnetic field (nuclear field $\boldsymbol{B}_{\mathrm{n}}$) opposite to the applied magnetic field, modulating the spin transfer rate from the electron to lattice nuclei. More recently, double bistability has been observed in single InAlAs QDs as a result of the modulated spin transfer rate due to nuclear spin fluctuation, which implies the presence of *tristablity* of the NSP [11,12].

Because it is possible to lower the spin temperature using dynamical nuclear polarization, a special technique has been used to concentrate the population into a single nuclear state [13]. Therefore the optically detected NMR technique has been realized in individual QDs, revealing some important properties of the QD spin system, such as the hyperfine constant and strain distributions. Furthermore, this strategy is expected to realize quantum information processing stored in QD nuclear spins even if there exist only few tens of thousands of nuclei in a single QD [3].

While NSP is associated with many interesting phenomena and applications, nuclear quadrupole interaction (NQI) has received significant attention recently. In QDs grown by a strain-driven process, it has been pointed out that NQI induced by the residual strain is crucial for describing the spin dynamics of electron-nuclei (e-n) coupled system. For example, the mixing of nuclear spin states caused by NQI enhances the decay process of NSP [14–16]. In addition, noncollinear HFI arising from NQI is responsible for the bidirectional NSP observed as a *dragging effect* in absorption spectra [17,18] and utilized to create many-body coherences and access the collective quantum memories [2,19,20]. Further, NQI has a significant impact on the electron decoherence process through HFI, resulting in more complex spin dynamics [21,22].

Formation of a large $\boldsymbol{B}_{\mathrm{n}}$ perpendicular to a photo-injected electron spin under a transverse magnetic field, known as the *anomalous Hanle effect*, is a remarkable phenomenon [23–26]. This phenomenon has not been observed in strain-free systems, such as bulk [27] and QDs grown by droplet epitaxy [28]. This strongly suggests that the strain-induced NQI plays an important role in the generation of the anomalous Hanle effect. Thus studying the anomalous Hanle effect may not only provide useful insight into NQI but also pave the way to utilize NSP in semiconductor nanostructures with more accuracy and wide range of control.

So far, the anomalous Hanle effect has only been studied regarding time-integrated measurements of photoluminescence (PL) from single QDs. Without a nuclear field, the Hanle curve has a Lorentzian shape, and its width, which is essentially determined by the electron spin lifetime and g factor, is expected to be tens to hundreds of milli-Tesla for

[*]Present address: Department of Materials Science, Tohoku University, 6-6-02, Aramaki-aza Aoba, Aoba-ku, Sendai 980-8579, Japan.
[†]r-kaji@eng.hokudai.ac.jp
[‡]adachi-s@eng.hokudai.ac.jp

 ©2023 American Physical Society

typical QDs. However, under the anomalous Hanle effect, the width turned out to be 10 times larger than expected. This observation is interpreted as the applied transverse field being compensated by the generated in-plane component of nuclear field ($B_{n,x}$). Moreover, note that a gradual decay of the longitudinal component of nuclear field ($B_{n,z}$) in the subtesla region was observed. This is contrary to the model based on spin-cooling theory [27], which predicts that $B_{n,z}$ disappears under an applied transverse magnetic field exceeding the dipolar field among nuclei.

In a previous study [25], we developed a phenomenological model for the anomalous Hanle effect, assuming the following two points: the stabilization effect of NSP on the sample growth axis (z axis) and large anisotropy of the hyperfine constant. The stabilization effect is attributed to the fact that the major principal axis of NQI aligns with the z axis [29], which was widely accepted at the time. Further, to explain the observations, the model had to include a somewhat significant assumption that the hyperfine constant experiences a sign change for the in-plane (x and y) and out-of-plane (z) components. The model successfully explains the formation of $B_{n,x}$ and gradual decay of $B_{n,z}$, but does not consider the tilt of NQI major principal axis [30]. In particular, Huang *et al.* [31] studied magneto-optical anomalies associated with NQI in various symmetry-lowered InGaAs QD structures and convincingly demonstrated that the major principal axis of NQI is generally not along the z axis resulting in the permanent in-plane nuclear field. They further noted that they did not detect a large anisotropy in the hyperfine constant. To clarify the role that the tilted major principal axis plays in the anomalous Hanle effect and revise our previous model, we performed time-resolved measurements of PL from a single QD.

In this paper, we study the anomalous Hanle effect from both experimental and theoretical aspects. Based on the measurements taken in time domain, we found that the buildup time of nuclear field increased with increasing the applied transverse magnetic field. Furthermore, the circular polarization degree of PL was reversed within a timescale three orders of magnitude faster than the nuclear field buildup time, when the helicity of excitation light was reversed. This fast response to the change of excitation helicity led us to reconsider the previous model of the anomalous Hanle effect. The model proposed in this study clarifies that the essential requirement for NQI to explain the anomalous Hanle effect is the presence of the in-plane component of the major principal axis.

II. EXPERIMENTS

The sample was single $In_{0.75}Al_{0.25}As/Al_{0.3}Ga_{0.7}As$ self-assembled (SA) QDs grown by molecular beam epitaxy on a (001)-GaAs substrate. Mesa fabrications reduced the areal density of QD and enabled us to access PL from individual QDs. Typical PL spectra obtained from a single QD are shown in Fig. 1. We focused only on the PL from a positively charged exciton (X^+) because the degree of circular polarization (DCP denoted as ρ_c) of X^+ PL is proportional to the electron spin polarization $\langle S_z \rangle$ [32]. Throughout this study, the following definition is used: $\rho_c = (I^- - I^+)/(I^- + I^+)$, where $I^\pm$ is the intensity of $\sigma^\pm$ polarized PL. This leads to the following relation: $\langle S_z \rangle = \rho_c/2$.

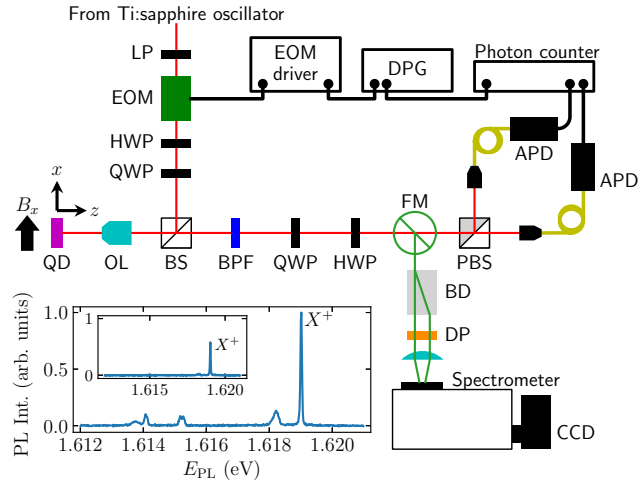

FIG. 1. Schematics of the measurement system. LP: linear polarizer. FM was used to switch between time-resolved and time-integrated PL measurements. The bottom panel shows the PL spectra obtained from a single QD (E_{PL}: PL energy). A band-pass filter (BPF) allowed us to extract only X^+ PL peak as depicted in the inset.

Figure 1 shows the schematics of the measurement system. Excitation light was provided by a cw-Ti:sapphire oscillator whose wavelength was tuned to the wetting layer of our InAlAs QDs (~730 nm). A half-wave plate (HWP) and quarter-wave plate (QWP) were used to control the excitation polarization. The set of waveplates also corrects the optical phase distortion caused by the optical elements such as mirrors and beam splitters (BSs). Further, an electro-optic modulator (EOM) in the excitation path was used to rapidly switch the light polarizations.

The sample was cooled to 6 K in a cryostat installed in a superconducting magnet, which provided a static magnetic field in the sample growth plane (xy). Hereafter, B_x stands for the applied transverse magnetic field. The excitation light was focused onto the sample surface through an objective lens (OL) along the z axis, and PLs were collected through the same OL in reflection geometry. The spot size of the laser on the sample surface was ~2 μm. The excitation power for each measurement was set so that the X^+ PL intensity is saturated.

In the detection path, σ^+ and σ^- components of X^+ PL were converted to mutually orthogonal linearly polarized pairs (π^x, π^y) by a QWP. These polarization-converted PL components were observed by different detectors depending on the types of measurements, namely, time-integrated or time-resolved. This selection was made using a flipper mirror (FM).

In the time-integrated measurements, the two orthogonal PL polarizations were spatially separated by a beam displacer (BD). These PL components were then dispersed by a triple grating spectrometer, and finally, were simultaneously accumulated at different regions of a liquid N_2-cooled Si-charge coupled device (Si-CCD) with an integration time of 1 second. A depolarizer (DP) placed just after BD was used to eliminate the difference in diffraction efficiency between π^x and π^y in the spectrometer.

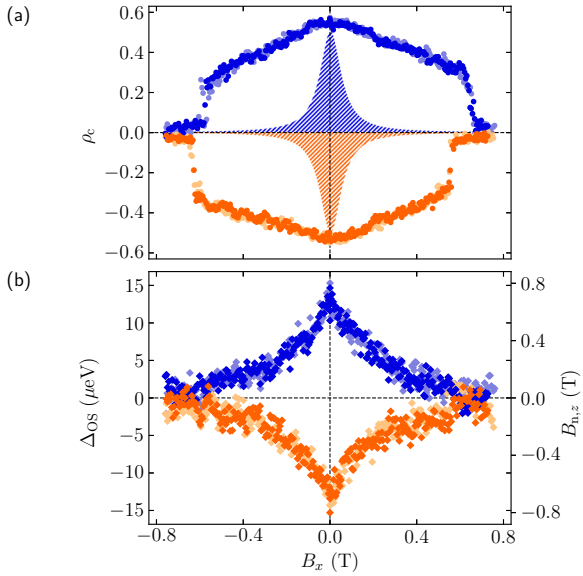

FIG. 2. (a) Time-integrated measurements of anomalous Hanle curves in a single InAlAs SAQD under σ^- (blue) and σ^+ (orange) excitations. The dark (light) markers indicate the data obtained with increasing (decreasing) B_x. Hatched regions indicate the Hanle curves where $|\boldsymbol{B}_n| = 0$. (b) Δ_{OS} as a function of B_x. Right axis corresponds $B_{n,z}$ deduced from $B_{n,z} = \Delta_{OS}/(g_e \mu_B)$.

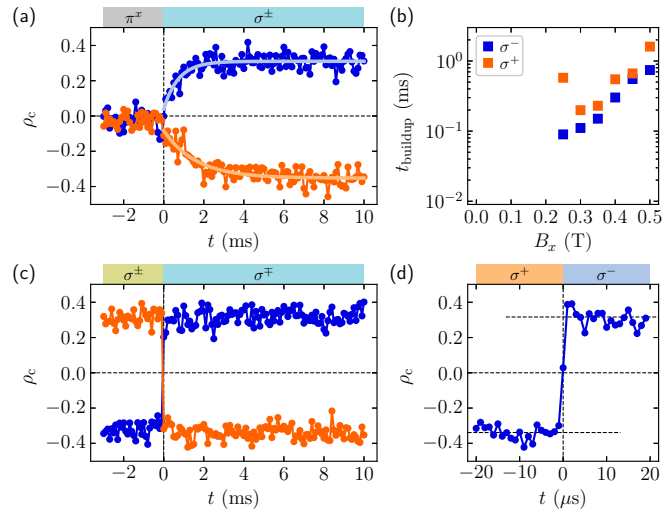

FIG. 3. (a) Temporal evolutions of ρ_c with respect to the switching of excitation polarization $\pi^x \rightarrow \sigma^\pm$ at $t = 0$. When $t > 0$, blue and orange markers indicate data under σ^- and σ^+ excitations, respectively. (b) B_x dependence of $t_{buildup}$. Blue (orange) squares indicate the case under $\sigma^{-(+)}$ excitation when $t > 0$. (c) Temporal evolution of ρ_c with respect to the switching of excitation helicity; orange (blue) markers indicate the case with $\sigma^{-(+)} \rightarrow \sigma^{+(-)}$ at $t = 0$. (d) The transition of ρ_c in the fast time range of $|t| < 20$ μs in the case of $\sigma^+ \rightarrow \sigma^-$ at $t = 0$. The data shown in (a), (c), and (d) were obtained at $B_x = 0.5$ T.

In the time-resolved measurements, the X^+ PL was energetically selected using a band-pass filter (BPF) with a transmission bandwidth of 0.5 nm. The inset of the bottom panel depicted in Fig. 1 shows the PL after the BPF whose transmission band was tuned to X^+ emission. As shown in this figure, PL lines other than that originating from X^+ were effectively suppressed. After this extraction, the two orthogonal linearly polarized components converted from σ^+ and σ^- were spatially resolved by a polarizing beam splitter (PBS). Subsequently, these were detected by avalanche photodiodes (APDs); accordingly, incident photons in each APD were counted by a two-channel photon counter. A delayed pulse generator (DPG) was connected to the counter and the EOM driver to synchronize the gate timing of the counter with the excitation polarization switching.

Figures 2(a) and 2(b) show the B_x dependencies of ρ_c and the Overhauser shift Δ_{OS} observed in the time-integrated measurements for a target single QD, where the excitation power was ∼125 μW. Here, Δ_{OS} works as a measure of $B_{n,z}$ through the relation $\Delta_{OS} = g_e \mu_B B_{n,z}$, where g_e and μ_B are the electron g factor and Bohr magneton, respectively. Δ_{OS} is evaluated directly as the energy splitting between σ^+ and σ^- PL peaks and given by $\Delta_{OS} = E^- - E^+$, where $E^\pm$ denotes the PL energy of $\sigma^\pm$ component. The hatched regions depicted in Fig. 2(a) indicate the calculated Hanle curves without a nuclear field. The calculated curve is a Lorentz function of B_x with the half width of $B_{1/2} = \hbar/(|g_e|\mu_B \tau_e)$, where $\hbar$ is the reduced Planck constant and τ_e is the electron spin lifetime. For this calculation, $|g_e| = 0.39$ and $\tau_e = 0.5$ ns were used; the former was a measured value and latter was an estimation for a typical QD.

The observed Hanle curves had a significant width compared to that of the hatched region. In addition, sudden changes in ρ_c appeared around $|B_x| \sim 0.6$ T, which were accompanied by hysteresis [23–25]. Further, as shown in Fig. 2(b), Δ_{OS} decreased quite slowly as $|B_x|$ increased. These behaviors could not be explained by the traditional model [27] where the modulation of Hanle curve occurs only within the weak magnetic field region of $|B_x| \lesssim B_{1/2}$ and large $B_{n,z}$ can be maintained only within a weak magnetic field region of $\sim 10^{-1}$ mT.

To complement the time-integrated measurements regarding the formation process of the in-plane nuclear field, the time-resolved PL measurements of ρ_c under B_x were performed. Figure 3(a) shows the temporal evolution of ρ_c at $B_x = 0.5$ T where large DCPs have been observed in the time-integrated measurements [Fig. 2(a)]. In Fig. 3(a), the excitation power was ∼175 μW and excitation polarization was set to π^x in negative time region ($t < 0$) and switched to $\sigma^\pm$ at $t = 0$. The observed DCPs under σ^- and σ^+ excitations are indicated by blue and orange markers, respectively. After fitting with a single exponential function, a buildup time of ρ_c, $t_{buildup}$, under $\sigma^{-(+)}$ excitation was evaluated as 0.7 (1.6) ms. B_x dependence of $t_{buildup}$ is summarized in Fig. 3(b). Regardless of the excitation polarization, $t_{buildup}$ increased with increasing B_x.

The NSP for $t < 0$ is considered to be zero because π^x excitation injects spin-balanced electron, i.e., $\langle S_z \rangle = 0$. On the other hand, $\sigma^\pm$ excitation for $t > 0$ resulted in an increase in $\boldsymbol{B}_n$ owing to spin-selective injection of electrons. Because the compensation of B_x by $B_{n,x}$ should suppress the electron spin precession, the change in $|\rho_c|$ reflects the increase in $\boldsymbol{B}_n$. Indeed, Fig. 3(a) shows that $|\rho_c|$ has increased from zero at

$t = 0$ to the steady-state value of ∼0.4. Thus Fig. 3(b) implies that the buildup time of $B_{n,x}$ increased with increasing B_x. In this context, additionally, the difference in $t_{buildup}$ between σ^+ and σ^- excitation cases could be attributed to the unintentional displacement of the applied magnetic field from the xy plane, which breaks the symmetry of spin-flip process [33].

Figure 3(c) shows the temporal evolution of ρ_c when the excitation light was circularly polarized at $t < 0$ and switched to counter polarized ($\sigma^{\pm} \rightarrow \sigma^{\mp}$) at $t = 0$. The excitation power and B_x were set to ∼175 μW and 0.5 T, respectively. The large $|\rho_c|$ for $t < 0$ is considered as a result of steady-state $B_{n,x}$ compensating for B_x because the excitation duration for $t < 0$ was set to 5 ms, which is sufficiently longer than $t_{buildup}$. As clearly shown, the observed ρ_c reverses its sign while maintaining its magnitude of ∼0.4 after the switching of excitation helicity at $t = 0$. Further, the sign reversal of ρ_c was completed within 1 μs as depicted in Fig. 3(d); the response was at least three orders of magnitude faster than $t_{buildup}$.

III. ALTERNATIVELY DEVELOPED MODEL

A. Failure of previously proposed model

According to the previous model for the anomalous Hanle effect observed in time-integrated measurements [25], we computed the temporal evolution of the electron and nuclear spins in a QD and compared the results with the experimental data.

Figure 4(a) shows the computed temporal evolution of $\langle S_z \rangle$, $B_{n,x}$, and $B_{n,z}$ from the top panel down, respectively, under σ^- excitation for $t > 0$, which corresponds to the blue markers depicted in Fig. 3(a). In this figure, the horizontal axis is a logarithmic scale to depict the trace of these results over a wide range of time.

As clearly shown, $\langle S_z \rangle$ under nonzero B_x exhibits a significant increase. This change in $\langle S_z \rangle$ is due to the formation of $B_{n,x}$ as shown schematically in Fig. 4(c). The optically-injected electron spin polarization $\langle \boldsymbol{S}_0 \rangle$ is transferred to the nuclear spin system by the e-n flip-flop process due to HFI. As a result, the z component of NSP and resultant $B_{n,z}$, which are stabilized by NQI whose major principal axis is along the z axis, appear in the same direction with $\langle S_z \rangle$. Thus the torque vector of electron spin precession, which is parallel to the total effective field $\boldsymbol{B}_T$ seen from the electron, is tilted in the zx plane, and the electron spin polarization $\langle \boldsymbol{S} \rangle$ acquires a nonprecessing component along the x axis, $\langle S_x \rangle$. The direction of $\boldsymbol{B}_T$ changes as $B_{n,x}$ grows. Finally, $\langle S_x \rangle$ contributes the formation of $B_{n,x}$, which is orthogonal to $\langle \boldsymbol{S}_0 \rangle$ and compensates for B_x.

As represented by the blue squares in Fig. 4(d), the buildup time of computed $\langle S_z \rangle$, $t_{buildup}$, in which $\langle S_z \rangle$ reaches the saturated value, becomes longer as B_x increases. Therefore the overall behaviors regarding to the formation dynamics of $B_{n,x}$ are qualitatively consistent with the experimental results shown in Figs. 3(a) and 3(b).

Figure 4(b) shows the computed temporal evolution of $\langle S_z \rangle$, $B_{n,x}$, and $B_{n,z}$ from the top panel down, respectively, after switching the excitation polarization from σ^- to σ^+ at $t = 0$, which corresponds to the orange markers depicted in Fig. 3(c). After a change in sign, $\langle S_z \rangle$ represents a *dent structure*, that

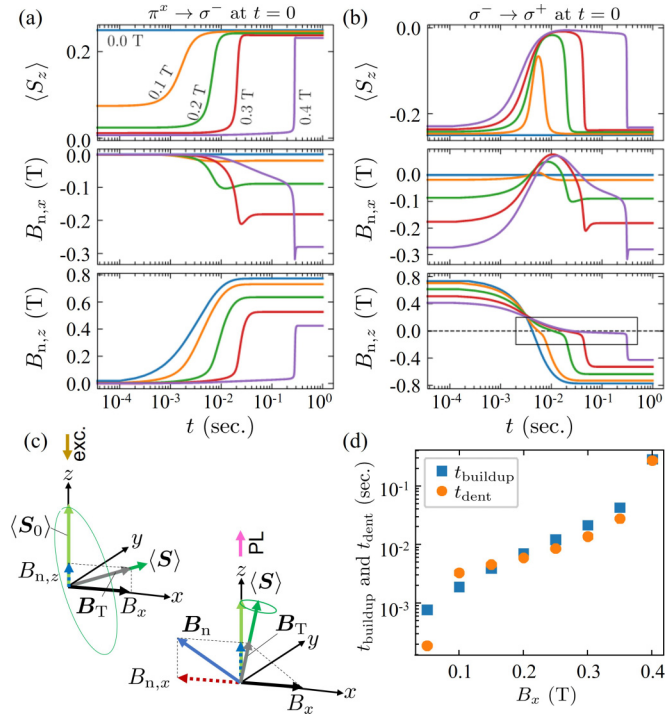

FIG. 4. Computed results of the dynamical changes in $\langle S_z \rangle$, $B_{n,x}$, and $B_{n,z}$ based on the previously proposed model [25]. B_x was varied from 0 to 0.4 T. (a) and (b) depict the temporal evolutions of $\langle S_z \rangle$ (top panel), $B_{n,x}$ (middle), and $B_{n,z}$ (bottom) after the switching of $\pi^x \rightarrow \sigma^-$ and $\sigma^- \rightarrow \sigma^+$ at $t = 0$, respectively. (c) The configuration of electron spin polarization $\langle \boldsymbol{S} \rangle$, $\boldsymbol{B}_n$, and B_x. The left side shows the initial state in which $B_{n,z}$ begins to emerge, and the right side shows the final state in which $B_{n,x}$ that compensates for B_x occurs. Here, $\boldsymbol{B}_T$ is a total effective magnetic field seen from the perspective of an electron, and $\langle \boldsymbol{S}_0 \rangle$ is the initial value of $\langle \boldsymbol{S} \rangle$. (d) B_x dependencies of $t_{buildup}$ (squares) and t_{dent} (circles).

is, an abrupt drop in $|\langle S_z \rangle|$ is followed by a recovery to the saturated value. The width of the dent, t_{dent}, defined as the time duration in which $|\langle S_z \rangle|$ is less than $1/e$ of the saturated value, increases with increasing B_x as plotted by orange circles in Fig. 4(d).

Further, t_{dent} is of the same order of magnitude as $t_{buildup}$, suggesting that t_{dent} is also determined by the dynamics of NSP. In particular, the dent structure originates from the transient process of $B_{n,z}$ in this model. As shown in the bottom panel of Fig. 4(b), after switching of the excitation helicity, $|B_{n,z}|$ starts to decrease, passes through zero, and reaches the saturated value with the opposite sign. During this process, a time period emerges where $B_{n,x}$ is not strong enough to cancel out the applied transverse magnetic field [middle panel of Fig. 4(b)], while $|B_{n,z}|$ is kept near zero as indicated by the square in the bottom panel. During this time period, $|\langle S_z \rangle|$ is kept small because the electron spin experiences a large transverse field. In this model, therefore, the slow evolution of $B_{n,z}$ is responsible for the dent structure indicating $t_{dent} \sim t_{buildup}$. However, in the experimental results depicted in Figs. 3(c) and 3(d), the change in ρ_c occurred over a time span three orders of magnitude faster than $t_{buildup}$, and no dent structures were observed. This discrepancy, which was revealed for the first

time in time-resolved measurements, motivated us to reconsider our previous model.

B. Description of alternative model

In this section, we provide an overview of the alternative model. The model assumes that the correlation among nuclei is neglected, and thus, the state of individual nucleus is described only by its population of eigenstate. Therefore the spin polarization of jth nucleus is given by

$$\langle \boldsymbol{I}_j \rangle = \sum_{m_j} P_{m_j} \langle m_j | \hat{\boldsymbol{I}}_j | m_j \rangle, \tag{1}$$

where P_{m_j} is the population probability of the eigenstate $|m_j\rangle$ with eigenenergy $\epsilon_{\mathrm{n},m_j}$. The interaction, which determines the eigenstates of nucleus, is the sum of Zeeman interaction and NQI, and the corresponding spin Hamiltonians, $\mathscr{H}^{(\mathrm{n})}_{\mathrm{Z},j}$ and $\mathscr{H}_{\mathrm{Q},j}$, are expressed as

$$\mathscr{H}^{(\mathrm{n})}_{\mathrm{Z},j} = \left(-\mathrm{g}_{\mathrm{n},j}\mu_{\mathrm{N}}\boldsymbol{B} + f_{\mathrm{e}}\frac{2A_j}{N}\langle \boldsymbol{S} \rangle \right) \cdot \hat{\boldsymbol{I}}_j, \tag{2}$$

$$\mathscr{H}_{\mathrm{Q},j} = \frac{\mathrm{g}_{\mathrm{n},j}\mu_{\mathrm{N}}B_{\mathrm{Q},j}}{2}\left(\hat{I}^2_{\mathrm{Z},j} - \frac{I_j(I_j+1)}{3} \right). \tag{3}$$

Here, μ_{N} is the nuclear magneton, $\mathrm{g}_{\mathrm{n},j}$ is nuclear g factor, $\boldsymbol{B}$ is the external magnetic field, f_{e} is a temporal fraction in which unpaired electron spins occupy the localization volume, A_j is the hyperfine constant, N is the number of nuclei in the localization volume of electron, and $B_{\mathrm{Q},j}$ is the reduced energy of NQI in terms of magnetic field strength. $\hat{\boldsymbol{I}}_j$ is the spin operator of jth nucleus and $\hat{I}_{\mathrm{Z},j}$ is the component along the major principal axis of NQI (q axis). Note that $\mathscr{H}^{(\mathrm{n})}_{\mathrm{Z},j}$ includes the effect of Knight field through the second term of Eq. (2), which assumes a spatially uniform electron wave function with a probability amplitude of $\sqrt{2/(v_0 N)}$, where v_0 denotes the unit cell volume.

On the other hand, because the dynamics of electron spin is faster enough to be neglected compared to that of nuclear spins, the electron spin state is described as a steady state of the Bloch equation:

$$\langle \boldsymbol{S} \rangle = \frac{[(\boldsymbol{\omega}_{\mathrm{e}}\tau_{\mathrm{e}}) \cdot \langle \boldsymbol{S}_0 \rangle](\boldsymbol{\omega}_{\mathrm{e}}\tau_{\mathrm{e}}) + (\boldsymbol{\omega}_{\mathrm{e}}\tau_{\mathrm{e}}) \times \langle \boldsymbol{S}_0 \rangle + \langle \boldsymbol{S}_0 \rangle}{1 + (\omega_{\mathrm{e}}\tau_{\mathrm{e}})^2}. \tag{4}$$

Here, $\boldsymbol{\omega}_{\mathrm{e}}$ is a torque vector of Larmor precession given by

$$\boldsymbol{\omega}_{\mathrm{e}} = \frac{\mathrm{g}_{\mathrm{e}}\mu_{\mathrm{B}}(\boldsymbol{B} + \boldsymbol{B}_{\mathrm{n}})}{\hbar}. \tag{5}$$

Similar to the Knight field, assuming the spatially uniformity of the electron wave function, $\boldsymbol{B}_{\mathrm{n}}$ is written as

$$\boldsymbol{B}_{\mathrm{n}} = \sum_j \frac{2A_j}{\mathrm{g}_{\mathrm{e}}\mu_{\mathrm{B}}N}\langle \boldsymbol{I}_j \rangle. \tag{6}$$

The temporal evolution of spin-coupled system is given by the equation of motion for P_{m_j} as follows

$$\frac{dP_{m_j}}{dt} = \sum_{n_j,\varphi,\psi} \left(W_{m_j;\varphi,n_j;\psi}P_{n_j} - W_{n_j;\psi,m_j;\varphi}P_{m_j} \right). \tag{7}$$

Here, $W_{m_j;\varphi,n_j;\psi}$ is the transition rate from a direct product state $|n_j\rangle|\psi\rangle$ to $|m_j\rangle|\varphi\rangle$ where $|m_j(n_j)\rangle$ and $|\varphi(\psi)\rangle$ stand for the spin eigenstates of a nucleus and electron, respectively. The electron spin state satisfies

$$(\hat{\boldsymbol{S}} \cdot \boldsymbol{n})|\varphi\rangle = S_\varphi|\varphi\rangle, \tag{8}$$

where $\hat{\boldsymbol{S}}$ is electrons spin operator, $\boldsymbol{n} = \langle \boldsymbol{S} \rangle / |\langle \boldsymbol{S} \rangle|$ and $S_\varphi = \pm 1/2$.

In our model, only HFI and a phenomenologically introduced relaxation process drive the transitions among nuclear spin states. The transition rate due to HFI is written as

$$W^{\mathrm{HFI}}_{m_j;\varphi,n_j;\psi} = f_{\mathrm{e}}D_\psi \frac{2\delta_{\mathrm{c}}}{\hbar} \frac{|\langle m_j|\langle\varphi|\mathscr{H}_{\mathrm{HFI},j}|n_j\rangle|\psi\rangle|^2}{\delta^2_{\mathrm{c}} + (\epsilon_{m_j;\varphi} - \epsilon_{n_j;\psi})^2}, \tag{9}$$

where $\delta_{\mathrm{c}} = \hbar/\tau_{\mathrm{c}}$ represents a broadening of the state determined by a correlation time τ_{c} of HFI [7,34]. Moreover $\mathscr{H}_{\mathrm{HFI},j}$ is the Hamiltonian of HFI between jth nucleus and electron given by

$$\mathscr{H}_{\mathrm{HFI},j} = \frac{2A_j}{N}\hat{\boldsymbol{I}}_j \cdot \hat{\boldsymbol{S}}, \tag{10}$$

$D_\psi = (1 + 2S_\psi|\langle \boldsymbol{S} \rangle|)/2$ is the probability that the electron spin takes state $|\psi\rangle$, and $\epsilon_{m_j,\varphi} = \epsilon_{\mathrm{n},m_j} + \epsilon_\varphi$ is the energy of spin state $|m_j\rangle|\varphi\rangle$. Here, $\epsilon_\varphi = \langle\varphi|\mathscr{H}_{\mathrm{e}}|\varphi\rangle$ is the energy of electron spin state $|\varphi\rangle$ and is determined by

$$\mathscr{H}_{\mathrm{e}} = \left(\mathrm{g}_{\mathrm{e}}\mu_{\mathrm{B}}\boldsymbol{B} + \sum_j \frac{2A_j}{N}\langle \boldsymbol{I}_j \rangle \right) \cdot \hat{\boldsymbol{S}}, \tag{11}$$

which is the Zeeman Hamiltonian for $\boldsymbol{B}$ and $\boldsymbol{B}_{\mathrm{n}}$.

The phenomenological relaxation term is simply described by a single parameter γ_{d}, namely, the relaxation rate of nuclear spin, which is written as

$$W^{\mathrm{d}}_{m_j;\varphi,n_j;\psi} = -\gamma_{\mathrm{d}}. \tag{12}$$

This connects all eigenstates of nucleus equivalently and leads to a single exponential decay of macroscopic NSP with a characteristic time of $T_{\mathrm{ND}} = [(2I+1)\gamma_{\mathrm{d}}]^{-1}$. This term may originate from the following: the dipolar coupling among nuclei [27], indirect coupling via HFI [35], spin diffusion into the vicinity of QD [36,37], or something agitating the nuclear spin system even if the NQI is absent [38].

While A_j was treated as a tensorlike parameter whose components have a large anisotropy in the previous model [25], we now regard it as isotropic. Namely, A_j implemented in Eqs. (2), (6), (10), and (11) is a scalar quantity in the alternatively developed model. This is a significant deviation from the previous model.

In the following computations, these assumed values for InAlAs QDs are used: $\mathrm{g}_{\mathrm{n}} = +1.0$, $A_j = \tilde{A} = 50$ μeV, $N = 3\times10^4$, $f_{\mathrm{e}} = 0.015$, $\tau_{\mathrm{c}} = 50$ ps, $T_{\mathrm{ND}} = 100$ ms, $\mathrm{g}_{\mathrm{e}} = +0.35$, and $\tau_{\mathrm{e}} = 0.5$ ns. Note that the averaged value of hyperfine constant $\tilde{A}$ is used below for simplicity, although A_j depends on the nuclear species and is nonuniform in a practical system. The computations also assume that the g factor of electron spin in conduction band is isotropic, which has been confirmed both experimentally [25] and theoretically [39].

C. Reproduction of the observed temporal evolutions

As justified in the next subsection, the observed in-plane nuclear field formation can be reproduced by only considering

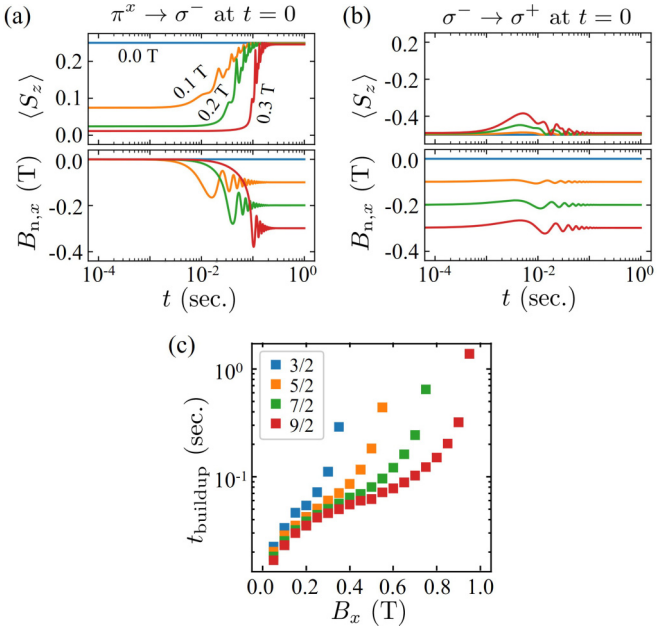

FIG. 5. [(a) and (b)] Temporal evolutions of $\langle S_z \rangle$ (top) and $B_{n,x}$ (bottom) with respect to the switching of $(\pi^x \rightarrow \sigma^-)$ and $(\sigma^- \rightarrow \sigma^+)$, respectively. B_x was varied from 0 to 0.3 T. In these computations, $I = 3/2$ and $B_Q = 0.3$ T are assumed. (c) B_x dependence of $t_{buildup}$ of $B_{n,x}$. Blue, orange, green, and red markers indicate the computed $t_{buildup}$ of $B_{n,x}$ with $I = 3/2$, $5/2$, $7/2$, and $9/2$, respectively. As shown in (a), the buildup time of $\langle S_z \rangle$ is in the same time scale. In these figures, the q axes of all nuclei are assumed to be contained in the xy plane.

the NQI for which the major principal axis contains the in-plane component. For the time being, we demonstrate here that the observed time-resolved results can be reproduced by assuming that the major principal axes of NQI of all nuclei are contained in the xy plane.

Figure 5(a) shows the computations about the temporal evolutions of $\langle S_z \rangle$ (top) and $B_{n,x}$ (bottom) after the switching of excitation polarization $\pi^x \rightarrow \sigma^-$ at $t = 0$. Here, all nuclei in the system have spin quantum number of $I = 3/2$, and the strength of NQI for these nuclei is given by $B_Q = 0.3$ T. This figure corresponds to the experimental data presented in Fig. 3(a). The temporal evolution of $\langle S_z \rangle$ is qualitatively the same in these figures, that is, $\langle S_z \rangle$ increases in a certain time region and reaches a saturation value. In addition, it has been clarified that the change in $\langle S_z \rangle$ is synchronized with the formation of $B_{n,x}$. Further, $B_{n,x}$ compensating for B_x appears without the previous assumption that the signs of the in- and out-of-plane components of the hyperfine constant are opposite.

Note that the oscillations present in the computed results were not observed experimentally. These oscillations come from the repetition of excessive growth and reduction of $B_{n,x}$; the overgrown nuclear field reduces $\langle S_z \rangle$, which in turn reduces the nuclear field itself. Through the repeated experience with such sequences, the system approaches the steady state. These oscillations might arise from an oversimplification of the nuclear spin decay term expressed by Eq. (12) [40].

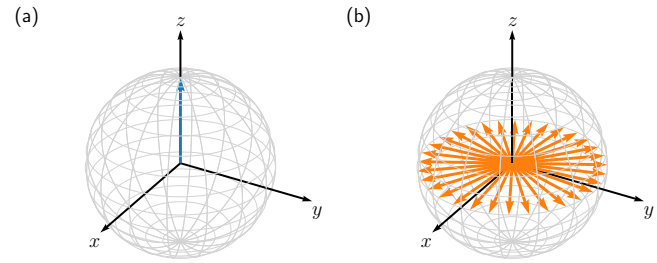

FIG. 6. Two limits of the major principal axis of NQI. (a) The q axes of all nuclei in a QD are along the z axis. (b) The q axes of individual nuclei are in the xy plane and uniformly distributed around the z axis.

The buildup time of $\langle S_z \rangle$, $t_{buildup}$, is summarized in Fig. 5(c). In the same figure, $t_{buildup}$ for the systems with $I = 5/2$, $7/2$, and $9/2$ are also plotted. The fact that the computed $t_{buildup}$ slows down as B_x increases is similar with the results presented in Fig. 3(b), while $t_{buildup}$ obtained from the computations are more than an order of magnitude slower than those obtained experimentally. Further, the nuclei with larger I tend to exhibit shorter $t_{buildup}$, that is, faster formation of $B_{n,x}$ even under a large B_x. From Eq. (10), HFI is stronger for the nuclear spin with larger I, which leads to an increase in the transition rate [Eq. (9)] that dominates the buildup time of NSP.

Figure 5(b) shows the computed temporal evolutions of $\langle S_z \rangle$ (top) and $B_{n,x}$ (bottom) after the switching of excitation polarization $\sigma^- \rightarrow \sigma^+$ at $t = 0$. The used line colors are the same as those used in Fig. 5(a). The results in the top panel should be compared with the observation depicted in Fig. 3(c). As clearly shown, the dent structure of $\langle S_z \rangle$, which appeared in the previous model [Fig. 4(b)], mostly disappears. This behavior agrees well with the experimental data. Therefore, by assuming the in-plane q axis, the alternatively developed model successfully reproduces the qualitative features of the experimental result obtained from the time-resolved measurements.

D. Relationship between directions of major principal axis of NQI and the generated nuclear field

In this section, we examine in more detail the requirement that the major principal axis of NQI contains the in-plane component, not the z component, for in-plane nuclear field formation. To verify the effect manifested by the in-plane component of q axis and that by the z component independently, we considered two limited situations shown in Fig. 6 and compared the computed steady states of the spin system.

At first, the situation where q axes of all nuclei being along the z axis [Fig. 6(a)] is considered. This situation has been frequently employed in previous research [14,18,41,42] with B_x being orthogonal to the q axis. The computed results of $\langle S_z \rangle$, $B_{n,x}$, and $B_{n,z}$ in the steady state are summarized in Fig. 7. Figure 7(a) shows the influence of the strength of NQI up to $B_Q = 1.5$ T where all nuclei in the system are assumed to be $I = 3/2$. On the other hand, Fig. 7(b) shows the difference in I from $3/2$ to $9/2$ with a constant NQI strength of $B_Q = 1.5$ T.

As shown in the top panel of Fig. 7(a), while *W-shaped* Hanle curve appears without NQI ($B_Q = 0.0$ T, blue curve),

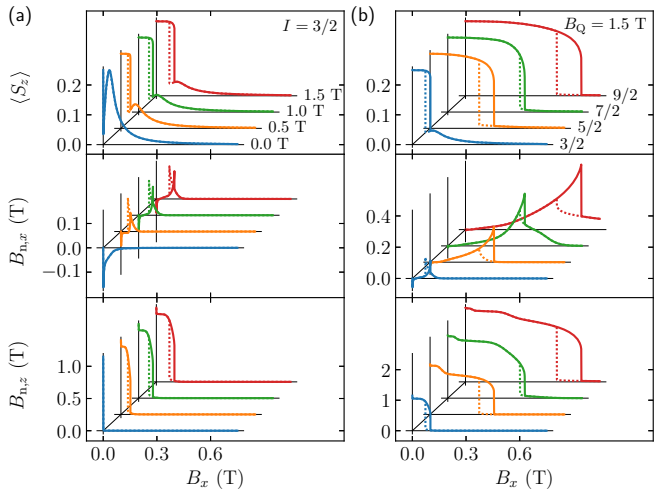

FIG. 7. The computed results of $\langle S_z \rangle$ (top), $B_{n,x}$ (middle), and $B_{n,z}$ (bottom) in the steady state of the system. Here, a q axis along z is assumed. Solid and dotted curves correspond to the results with increasing and decreasing B_x, respectively. (a) Dependencies on NQI strength B_Q for $I = 3/2$, where B_Q was varied from 0.0 to 1.5 T. (b) Difference in I from 3/2 to 9/2 at a constant $B_Q = 1.5$ T.

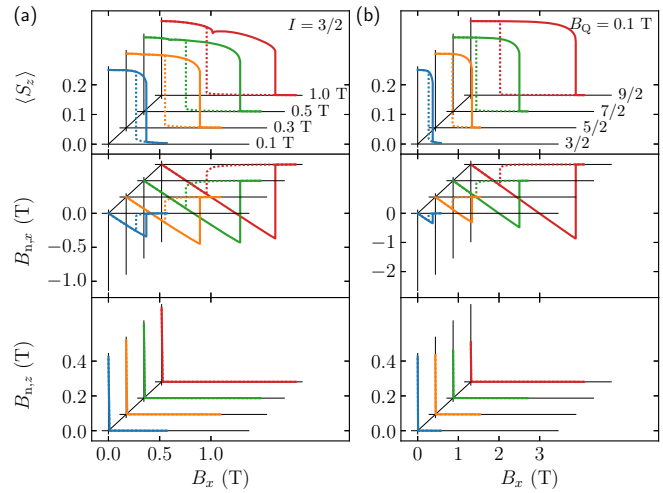

FIG. 8. The computed results of $\langle S_z \rangle$ (top), $B_{n,x}$ (middle), and $B_{n,z}$ (bottom) in the steady state of the system. The q axes for all nuclei are contained in the xy plane. Solid and dotted curves correspond to the results with increasing and decreasing B_x. (a) Dependencies on NQI strength B_Q on the computations for $I = 3/2$. B_Q was varied from 0.1 to 1.0 T. (b) Difference in I from 3/2 to 9/2 at a constant $B_Q = 0.1$ T.

the magnetic field region in which a large $\langle S_z \rangle$ is maintained expands with an increase of B_Q. Such a trend is commonly observed in systems with $I = 5/2$, 7/2, and 9/2 (not shown here). As shown in Fig. 7(b), an increment in I also expands the region where a large $\langle S_z \rangle$ is maintained.

Although these computed Hanle curves have a similar shape compared to that of the observed one, the expressed phenomenon is not the anomalous Hanle effect. This is because, the shape of the computed Hanle curve originates from B_x dependence of $B_{n,z}$. As shown in the bottom panels, a large $B_{n,z}$ appears even under a large B_x. This suggests that the NQI stabilizes the NSP in the direction of its major principal axis (z in this case) as considered phenomenologically in the previous studies [25,29]. The resultant large $B_{n,z}$ tilts the electron precession axis realizing a large $\langle S_z \rangle$. In fact, the change in $B_{n,z}$ is synchronized with the change in $\langle S_z \rangle$ in these figures.

Furthermore, as shown in the middle panels, $B_{n,x}$ with nonzero NQI has a positive value in the region $B_x > 0$. This means that $B_{n,x}$ is in the same direction as B_x, and the compensation of B_x by $B_{n,x}$ does not occur. This definitely contradicts the experimental results stated in a previous study [23]. Krebs *et al.* directly measured the Zeeman splitting of PL from single InAs/GaAs QDs and confirmed that B_x is compensated by $B_{n,x}$ when $\langle S_z \rangle$ shows a large value.

Next, the situation where the q axes for all nuclei are in the xy plane [Fig. 6(b)] is considered. Note that the q axes are assumed to be uniformly distributed in the xy plane. This is because the anomalous Hanle effect is observed regardless of the azimuth angle of the applied transverse field, and the effect of NQI is considered to have a cylindrical symmetry around the z axis [26]. The role of the in-plane component of q axis is included in the model by stating $\hat{I}_{Z,j} = \hat{I}_{x,j} \cos\phi_{Q,j} + \hat{I}_{y,j} \sin\phi_{Q,j}$ where $\phi_{Q,j}$ is the azimuth angle of q axis.

The computed steady states of $\langle S_z \rangle$, $B_{n,x}$, and $B_{n,z}$ are summarized in Fig. 8. Figure 8(a) compares the influence of the strength of NQI where all nuclei have the same spin of $I = 3/2$. On the other hand, Fig. 8(b) compares behaviors of the system depending on I with $B_Q = 0.1$ T.

As shown in the top panels, B_x dependence of $\langle S_z \rangle$, i.e., Hanle curve, deviates from a Lorentzian shape. Specifically, decrease in $\langle S_z \rangle$ is suppressed even under $|B_x| > B_{1/2}$ and thus the widths of Hanle curves are larger than the original, which is experimentally observed. The increase of B_Q or I results in an expansion of the magnetic field region in which a large $\langle S_z \rangle$ is maintained. Comparing the Hanle curves depicted in Fig. 8 with those depicted in Fig. 7, it can be seen that wider curves are formed even for a small B_Q. This also indicates that the in-plane component of the q axis has a significant impact on the anomalous Hanle effect.

Furthermore, from the middle panels of Fig. 8, it is found that the in-plane nuclear field is always formed in the opposite direction to the applied magnetic field. As long as such a nuclear field is formed, the effective transverse magnetic field experienced by the electron spin is kept small, and a large $\langle S_z \rangle$ is maintained. This means that the modulation of computed Hanle curves originates from the in-plane nuclear field opposite to the applied field. This situation agrees with the previously reported experimental results [23]. Accordingly, it is the in-plane component of the q axis that realizes the anomalous Hanle effect, namely, the formation of $B_{n,x}$ compensating B_x.

Nevertheless, the in-plane q axis cannot fully explain the entire experimental observation. As shown in the bottom panels of Fig. 8, the computed $B_{n,z}$ appears only within a small-B_x region, although the experimentally observed $B_{n,z}$ decays gradually over a wide range of B_x [Fig. 2(b)]. It has been reported theoretically [30] and experimentally [31] that the major principal axis of NQI is generally tilted from the z axis in actual QDs. Because the q axis contains both

the in-plane and z components, the anomalous Hanle effect and gradual decay of $B_{\mathrm{n},z}$, which arise from the different origins independently, are observed simultaneously. How the tilt angle of the q axis affects the computed steady states is summarized in Appendix B.

Note that the abrupt changes in computed $B_{\mathrm{n},z}$ values depicted in Fig. 7, which are not observed experimentally, are considered to arise from simplified assumptions that the parameters, such as B_{Q} and I, are treated as identical for all nuclei in the localization volume. The appropriate distributions of these parameters are necessary to reproduce the gradual decay of $B_{\mathrm{n},z}$ as observed.

IV. DISCUSSION

In the previous section, it was demonstrated that the in-plane component of q axis leads to the anomalous Hanle effect. The q axis being tilted and having an in-plane component is a plausible situation for actual QDs. In Ref. [30], Bulutay *et al.* have predicted such a large distribution of q axis by considering a large mixing of nuclear species in InGaAs QDs, which originates from the nuclear interdiffusion occurring during the growth process. A similar situation can be realized in our InAlAs/AlGaAs QDs through the same mechanism; several kinds of nuclei, such as In, Al, and As, exist in the localization volume of an electron. Further, Ga in the barrier layers may also contribute to the spin dynamics inside the localization volume because the interdiffusion can bring Ga into the QD and penetration of electronic wave function can expand the actual spatial region of the spin system into the barrier layer.

Note that such the homogeneous allocation of q axis depicted in Fig. 6 can be replaced by the nonzero biaxiality of NQI. This is because the role of this assumption is formally only for spin operators in the sample growth plane. The effect of the nonzero biaxiality of NQI is expressed by adding a term proportional to $\hat{I}_{X,j}^2 - \hat{I}_{Y,j}^2$ where $\hat{I}_{X,j}$ and $\hat{I}_{Y,j}$ are the spin operators of jth nucleus which observe spin expectation value orthogonal to each other and the q axis. Similar procedure has already been also applied in the symmetry-lowered InGaAs QD structures [31]. Thus the nonzero biaxiality of NQI could explain the anomalous Hanle effect, in which the q axis can be close to the z axis. As well as the deviation of the major principal axis, that of the biaxiality is also considered to deviate largely from zero [30].

Finally, we discuss the quantitativeness of t_{buildup}. As stated in the previous sections, the computed values of t_{buildup} are slower than the observed one. Recall here that the NSP has been described by treating HFI as a perturbation in the e-n spin coupled system [43], which determines the NSP formation rate roughly as $2f_{\mathrm{e}}\tau_{\mathrm{c}}[A/(\hbar N)]^2 I(I+1)/[S(S+1)]\langle S\rangle$. The shortest t_{buildup} of $\sim$5 μs is realized when spin $I = 9/2$ with $f_{\mathrm{e}} = 1$ and $\tau_{\mathrm{c}} \sim 1$ ns; this f_{e} is the theoretical upper limit, and τ_{c} is the longest value determined by the radiative lifetime of excitons. However, it has been observed that the actual value of f_{e} is in the order of 10^{-2} [14,15,35] and that of τ_{c} is few tens to hundreds of picoseconds [6,15,24,34]. Considering the actual situation, the theoretical value of t_{buildup} slows down to the order of a few milliseconds. The quantitative difference between the experimental and theoretical values of t_{buildup} may indicate either a failure of the weak coupling limit treating HFI just as a perturbation or other spin-driving forces, such as laser fields, need to be considered even under nonresonant excitation conditions [44].

V. CONCLUSION

In this study, time-resolved measurements of DCP of X^+ PL were performed to examine the spin dynamics of electron-nuclei coupled system in a single self-assembled InAlAs QD. The measurements revealed that the buildup time of the nuclear field increased as B_x was increased. In addition, the sign inversion of DCP was completed on a timescale at least three orders of magnitude faster than the nuclear field buildup time after the excitation helicity inversion. Based on this experimental result, we reconsidered our previous model [25], and succeeded in qualitatively reproducing the results observed in the time-resolved measurements as well as in the time-integrated measurements using the alternatively proposed model. In model computations, we verified the effects manifested owing to the in- and out-of-plane components of major principal axis of NQI *separately*. The in-plane nuclear field compensating the applied transverse field originates from the in-plane component of major principal axis, while the gradual decay of the longitudinal nuclear field originates from the component along the sample growth axis. These two effects arise from the different origins independently but are observed simultaneously. This is because the major principal axis of NQI in actual QDs is tilted from the sample growth axis and contains both in- and out-of-plane components.

ACKNOWLEDGMENT

We thank H. Sasakura for helpful discussions. We acknowledge the support of Japan Society for the Promotion of Science (20K03812 and 21H01745).

APPENDIX A: DETAILED DESCRIPTION OF THE PREVIOUSLY PROPOSED MODEL

The phenomenological model previously proposed in Ref. [25] qualitatively describes the anomalous Hanle effect in the steady state. The most striking feature of this model is the assumption that the hyperfine constant is highly anisotropic and has different signs for in- and out-of-plane components. As noted in the main text, this assumption is not included in the alternative model.

The nuclear spin systems can be separated into Zeeman-dominant and quadrupole-dominant systems, and the temporal evolution of these systems is treated independently by the following equations:

$$\frac{dI_{\mathrm{Z},\xi}}{dt} = -\frac{1}{T_{\mathrm{NF},\xi}}(\langle I_{\mathrm{Z},\xi}\rangle - \mathcal{Q}\langle S_\xi\rangle) - \frac{1}{T_{\mathrm{Z}}}\langle I_{\mathrm{Z},\xi}\rangle, \tag{A1}$$

$$\frac{dI_{\mathrm{Q},\xi}}{dt} = -\frac{1}{T_{\mathrm{NF},\xi}}(\langle I_{\mathrm{Q},\xi}\rangle - \mathcal{Q}\langle S_\xi\rangle) - \frac{1}{T_{\mathrm{Q}}}\langle I_{\mathrm{Q},\xi}\rangle. \tag{A2}$$

Here, $\mathcal{Q}$ is a material dependent scalar quantity and $\langle S_\xi\rangle$ is the electron spin polarization. $\langle I_{\mathrm{Z},\xi}\rangle$ ($\langle I_{\mathrm{Q},\xi}\rangle$) and T_{Z} (T_{Q}) are the nuclear spin angular momentum and NSP decay time in Zeeman (quadrupole)-dominant system, respectively. Similar

to other studies [6], the spin transfer rate from electron to nuclei is given by

$$\frac{1}{T_{\mathrm{NF},\xi}} = \frac{2f_e\tau_c(A_\xi/N)^2}{\hbar^2 + [g_{e,\xi}\mu_B(B_\xi + B_{n,\xi})\tau_c]^2}, \tag{A3}$$

where τ_c is the correlation time of the electron-nuclear coupled system.

Total nuclear spin polarization $\langle I_\xi \rangle$ seen from the electron spin as nuclear field is given by

$$\langle \boldsymbol{I} \rangle = (1 - r_Q)(\langle \boldsymbol{I}_Z \cdot \boldsymbol{b} \rangle)\boldsymbol{b} + r_Q(\langle \boldsymbol{I}_Q \rangle \cdot \boldsymbol{q})\boldsymbol{q}, \tag{A4}$$

where $\boldsymbol{b}$ and $\boldsymbol{q}$ are the unit vectors of the applied magnetic field and major principal axis of NQI, respectively. The effective magnetic field seen from nuclear spins is the sum of the applied field and Knight field originating from the electron spin polarization. The major principal axis of NQI implemented in this model is assumed to coincide with the z axis.

The reason why the contribution from each system is restricted to the corresponding direction is that the eigenstates of both Hamiltonians, the Zeeman interaction and quadrupole interaction, induce spin polarization at each quantization axis, even though only the occupancy of the eigenstates determines the nuclear spin state. Moreover, as B_x is increased, the relative strength of NQI decreases and nuclear eigenstates eventually converge to the eigenstates determined by the Zeeman Hamiltonian. Therefore the quadrupole-dominant system is considered to gradually disappear. This behavior is reflected in the parameter r_Q, which is defined as

$$r_Q = \frac{1}{1 + (B_x/B_Q)^2}. \tag{A5}$$

APPENDIX B: POLAR ANGLE DEPENDENCE

In the main text, we discussed the role of the in- and out-of-plane components of the major principal axis of NQI in the nuclear field formation process under the applied transverse magnetic field. Here, we consider a situation where the major principal axis of NQI is tilted.

Figure 9 shows the computed results for the steady state of the system under various values of θ_Q, considering $I = 3/2$ spins for simplicity. Here, θ_Q is the polar angle of the major principal axis of NQI with respect to the z axis. As shown in Fig. 9(b), when the major principal axis of NQI is close to z ($\theta_Q \sim 0^\circ$), the in-plane nuclear field ($B_{n,x}$) is in the same direction as the applied magnetic field (B_x). However, when the tilt of the major principal axis increases and θ_Q exceeds

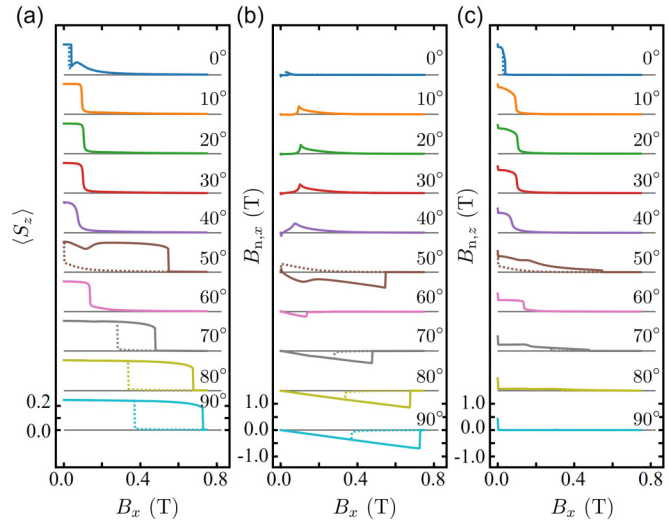

FIG. 9. The computed results of $\langle S_z \rangle$ (a), $B_{n,x}$ (b), and $B_{n,z}$ (c) in the steady state of the system under various values of the polar angle θ_Q of the NQI major principal axis. Solid and dashed lines denote the results for increasing and decreasing B_x, respectively. All nuclei are assumed to have a spin of 3/2, for simplicity.

60°, the in-plane nuclear field is generated in the opposite direction to the applied field, resulting in the compensation of B_x by $B_{n,x}$. Correspondingly, $\langle S_z \rangle$ shown in Fig. 9(a) maintains a large value even under a large B_x. This again indicates that the in-plane component of the major principal axis, clearly expressed in the main text, is key to the development of the anomalous Hanle effect.

On the other hand, as shown in Fig. 9(c), when the major principal axis of NQI contains a z component ($\theta_Q \neq 90^\circ$), a longitudinal nuclear field ($B_{n,z}$) appears and shows a nonzero value over a wide range of B_x even for $\theta_Q = 60 - 80^\circ$, where the tilt of the major principal axis is large. This reflects the fact that the expected value of the spin operator $\hat{I}_z$ for each nuclear spin eigenstate gets a nonzero value owing to the emergence of commutative part of $\hat{I}_z$ in the Hamiltonian that makes the expected value of $\hat{I}_z$ nonzero.

The boundary between the two regimes where the generated $B_{n,x}$ enhances or cancels out B_x is likely to exist around $\theta_Q = 50^\circ$. At this θ_Q angle, the sign of $B_{n,x}$ reverses when B_x is increased or decreased. That is, when B_x increases from 0 T, $B_{n,x}$ appears in the opposite direction of B_x, and when B_x decreases toward 0 T, $B_{n,x}$ appears in the same direction as B_x.

[1] J. M. Taylor, C. M. Marcus, and M. D. Lukin, Long-Lived Memory for Mesoscopic Quantum Bits, Phys. Rev. Lett. **90**, 206803 (2003).

[2] E. V. Denning, D. A. Gangloff, M. Atatüre, J. Mørk, and C. Le Gall, Collective Quantum Memory Activated by a Driven Central Spin, Phys. Rev. Lett. **123**, 140502 (2019).

[3] E. A. Chekhovich, S. F. C. da Silva, and A. Rastelli, Nuclear spin quantum register in an optically active semiconductor quantum dot, Nat. Nanotechnol. **15**, 999 (2020).

[4] S. Cortez, O. Krebs, S. Laurent, M. Senes, X. Marie, P. Voisin, R. Ferreira, G. Bastard, J.-M. Gérard, and T. Amand, Optically Driven Spin Memory in *n*-Doped InAs-GaAs Quantum Dots, Phys. Rev. Lett. **89**, 207401 (2002).

[5] H. Bluhm, S. Foletti, I. Neder, M. Rudner, D. Mahalu, V. Umansky, and A. Yacoby, Dephasing time of GaAs electron-spin qubits coupled to a nuclear bath exceeding 200 μs, Nat. Phys. **7**, 109 (2011).

[6] Recent optical investigation of nuclear spin physics in QDs are reviewed comprehensively: B. Urbaszek, X. Marie, T. Amand, O. Krebs, P. Voisin, P. Maletinsky, A. Högele, and A. Imamoglu, Nuclear spin physics in quantum dots: An optical investigation, Rev. Mod. Phys. **85**, 79 (2013).

[7] P.-F. Braun, B. Urbaszek, T. Amand, X. Marie, O. Krebs, B. Eble, A. Lemaître, and P. Voisin, Bistability of the nuclear polarization created through optical pumping in $In_{1-x}Ga_xAs$ quantum dots, Phys. Rev. B **74**, 245306 (2006).

[8] A. I. Tartakovskii, T. Wright, A. Russell, V. I. Fal'ko, A. B. Van'kov, J. Skiba-Szymanska, I. Drouzas, R. S. Kolodka, M. S. Skolnick, P. W. Fry, A. Tahraoui, H.-Y. Liu, and M. Hopkinson, Nuclear Spin Switch in Semiconductor Quantum Dots, Phys. Rev. Lett. **98**, 026806 (2007).

[9] P. Maletinsky, C. W. Lai, A. Badolato, and A. Imamoglu, Nonlinear dynamics of quantum dot nuclear spins, Phys. Rev. B **75**, 035409 (2007).

[10] R. Kaji, S. Adachi, H. Sasakura, and S. Muto, Hysteretic response of the electron-nuclear spin system in single $In_{0.75}Al_{0.25}As$ quantum dots: Dependences on excitation power and polarization, Phys. Rev. B **77**, 115345 (2008).

[11] S. Yamamoto, R. Kaji, H. Sasakura, and S. Adachi, Third stable branch and tristability of nuclear spin polarizations in a single quantum dot system, Phys. Rev. B **101**, 245424 (2020).

[12] S. Yamamoto, R. Kaji, H. Sasakura, and S. Adachi, Double nuclear spin switching in single quantum dots, Jpn. J. Appl. Phys. **60**, SBBH07 (2021).

[13] E. A. Chekhovich, A. Ulhaq, E. Zallo, F. Ding, O. G. Schmidt, and M. S. Skolnick, Measurement of the spin temperature of optically cooled nuclei and GaAs hyperfine constants in GaAs/AlGaAs quantum dots, Nat. Mater. **16**, 982 (2017).

[14] C.-W. Huang and X. Hu, Theoretical study of nuclear spin polarization and depolarization in self-assembled quantum dots, Phys. Rev. B **81**, 205304 (2010).

[15] O. Krebs, B. Eble, A. Lemaître, P. Voisin, B. Urbaszek, T. Amand, and X. Marie, Hyperfine interaction in InAs/GaAs self-assembled quantum dots: Dynamical nuclear polarization versus spin relaxation, C. R. Phys. **9**, 874 (2008).

[16] R. Matsusaki, R. Kaji, S. Yamamoto, H. Sasakura, and S. Adachi, Quadrupolar effect on nuclear spin depolarization in single self-assembled quantum dots, Appl. Phys. Express **11**, 085201 (2018).

[17] C. Latta, A. Högele, Y. Zhao, A. N. Vamivakas, P. Maletinsky, M. Kroner, J. Dreiser, I. Carusotto, A. Badolato, D. Schuh, W. Wegscheider, M. Atature, and A. Imamoglu, Confluence of resonant laser excitation and bidirectional quantum-dot nuclear-spin polarization, Nat. Phys. **5**, 758 (2009).

[18] A. Högele, M. Kroner, C. Latta, M. Claassen, I. Carusotto, C. Bulutay, and A. Imamoglu, Dynamic Nuclear Spin Polarization in the Resonant Laser Excitation of an InGaAs Quantum Dot, Phys. Rev. Lett. **108**, 197403 (2012).

[19] D. A. Gangloff, G. Éthier-Majcher, C. Lang, E. V. Denning, J. H. Bodey, D. M. Jackson, E. Clarke, M. Hugues, C. Le Gall, and M. Atatüre, Quantum interface of an electron and a nuclear ensemble, Science **364**, 62 (2019).

[20] D. A. Gangloff, L. Zaporski, J. H. Bodey, C. Bachorz, D. M. Jackson, G. Éthier-Majcher, C. Lang, E. Clarke, M. Hugues, C. Le Gall, and M. Atatüre, Witnessing quantum correlations in a nuclear ensemble via an electron spin qubit, Nat. Phys. **17**, 1247 (2021).

[21] N. A. Sinitsyn, Y. Li, S. A. Crooker, A. Saxena, and D. L. Smith, Role of Nuclear Quadrupole Coupling on Decoherence and Relaxation of Central Spins in Quantum Dots, Phys. Rev. Lett. **109**, 166605 (2012).

[22] R. Stockill, C. Le Gall, C. Matthiesen, L. Huthmacher, E. Clarke, M. Hugues, and M. Atatüre, Quantum dot spin coherence governed by a strained nuclear environment, Nat. Commun. **7**, 12745 (2016).

[23] O. Krebs, P. Maletinsky, T. Amand, B. Urbaszek, A. Lemaître, P. Voisin, X. Marie, and A. Imamoglu, Anomalous Hanle Effect due to Optically Created Transverse Overhauser Field in Single InAs/GaAs Quantum Dots, Phys. Rev. Lett. **104**, 056603 (2010).

[24] J. Nilsson, L. Bouet, A. J. Bennett, T. Amand, R. M. Stevenson, I. Farrer, D. A. Ritchie, S. Kunz, X. Marie, A. J. Shields, and B. Urbaszek, Voltage control of electron-nuclear spin correlation time in a single quantum dot, Phys. Rev. B **88**, 085306 (2013).

[25] S. Yamamoto, R. Matsusaki, R. Kaji, and S. Adachi, In-plane nuclear field formation investigated in single self-assembled quantum dots, Phys. Rev. B **97**, 075309 (2018).

[26] S. Yamamoto, T. Arakawa, R. Matsusaki, R. Kaji, and S. Adachi, Influence of a Longitudinal Field on the Large In-Plane Nuclear Field Formation in Single Quantum Dots, Phys. Status Solidi B **257**, 1900381 (2020).

[27] *Optical Orientation*, edited by F. Meier and B. Zakharchenya, Modern Problems in Condensed Matter Sciences Vol. 8 (North-Holland, NewYork, 1984).

[28] G. Sallen, S. Kunz, T. Amand, L. Bouet, T. Kuroda, T. Mano, D. Paget, O. Krebs, X. Marie, K. Sakoda, and B. Urbaszek, Nuclear magnetization in gallium arsenide quantum dots at zero magnetic field, Nat. Commun. **5**, 3268 (2014).

[29] R. I. Dzhioev and V. L. Korenev, Stabilization of the Electron-Nuclear Spin Orientation in Quantum Dots by the Nuclear Quadrupole Interaction, Phys. Rev. Lett. **99**, 037401 (2007).

[30] C. Bulutay, E. A. Chekhovich, and A. I. Tartakovskii, Nuclear magnetic resonance inverse spectra of InGaAs quantum dots: Atomistic level structural information, Phys. Rev. B **90**, 205425 (2014).

[31] Y. Q. Huang, Y. Puttisong, S. Filippov, I. A. Buyanova, and W. M. Chen, Oblique Nuclear Quadrupole Interaction in Self-Assembled Structures Based on Semiconductor Quantum Dots, Phys. Rev. Appl. **14**, 044019 (2020).

[32] Although spin dynamics are determined by all charge states in the QD, it is sufficient to consider only the most significant contributing charge states to capture the basis of the observations. Further, the charge state with the highest PL intensity is considered to have the largest contribution to the spin dynamics.

[33] B. Eble, O. Krebs, A. Lemaître, K. Kowalik, A. Kudelski, P. Voisin, B. Urbaszek, X. Marie, and T. Amand, Dynamic nuclear polarization of a single charge-tunable InAs/GaAs quantum dot, Phys. Rev. B **74**, 081306(R) (2006).

[34] B. Urbaszek, P.-F. Braun, T. Amand, O. Krebs, T. Belhadj, A. Lemaître, P. Voisin, and X. Marie, Efficient dynamical nuclear polarization in quantum dots: Temperature dependence, Phys. Rev. B **76**, 201301(R) (2007).

[35] P. Maletinsky, A. Badolato, and A. Imamoglu, Dynamics of Quantum Dot Nuclear Spin Polarization Controlled by a Single Electron, Phys. Rev. Lett. **99**, 056804 (2007).

[36] M. N. Makhonin, A. I. Tartakovskii, A. B. Van'kov, I. Drouzas, T. Wright, J. Skiba-Szymanska, A. Russell, V. I. Fal'ko, M. S. Skolnick, H.-Y. Liu, and M. Hopkinson, Long nuclear spin polarization decay times controlled by optical pumping in individual quantum dots, Phys. Rev. B **77**, 125307 (2008).

[37] S. Adachi, R. Kaji, S. Furukawa, Y. Yokoyama, and S. Muto, Nuclear spin depolarization via slow spin diffusion in single InAlAs quantum dots observed by using erase-pump-probe technique, J. Appl. Phys. **111**, 103531 (2012).

[38] T. Belhadj, T. Kuroda, C.-M. Simon, T. Amand, T. Mano, K. Sakoda, N. Koguchi, X. Marie, and B. Urbaszek, Optically monitored nuclear spin dynamics in individual GaAs quantum dots grown by droplet epitaxy, Phys. Rev. B **78**, 205325 (2008).

[39] M. Kahraman and C. Bulutay, Electron ground state g factor in embedded InGaAs quantum dots: An atomistic study, Phys. Rev. B **103**, 115303 (2021).

[40] To reduce the computation load, only 32 azimuth angles of q axis are considered in this manuscript, as depicted in Fig. 6(b). Thus the q axes are placed at equal intervals of $2\pi/32$ rad. Further, these oscillations in Figs. 5(a) and 5(b) remain even if the number of q axis is changed. Thus they are not considered to be artificial arising from the regular distribution of q axes.

[41] E. A. Chekhovich, K. V. Kavokin, J. Puebla, A. B. Krysa, M. Hopkinson, A. D. Andreev, A. M. Sanchez, R. Beanland, M. S. Skolnick, and A. I. Tartakovskii, Structural analysis of strained quantum dots using nuclear magnetic resonance, Nat. Nanotechnol. **7**, 646 (2012).

[42] P. S. Sokolov, M. Y. Petrov, T. Mehrtens, K. Müller-Caspary, A. Rosenauer, D. Reuter, and A. D. Wieck, Reconstruction of nuclear quadrupole interaction in (In, Ga)As/GaAs quantum dots observed by transmission electron microscopy, Phys. Rev. B **93**, 045301 (2016).

[43] A. Abragam, *The Principle of Nuclear Magnetism* (Oxford University Press, Oxford, UK, 1961).

[44] E. A. Chekhovich, M. N. Makhonin, K. V. Kavokin, A. B. Krysa, M. S. Skolnick, and A. I. Tartakovskii, Pumping of Nuclear Spins by Optical Excitation of Spin-Forbidden Transitions in a Quantum Dot, Phys. Rev. Lett. **104**, 066804 (2010).